DOI 10.36146/2026_03_06

Analysis of center segregation induced by density changes and shrinkage cavities using a moving-slice model in continuous casting

J. Lee, S. Seo, W. Cho, E. Lee, J. Jo, K. Kim

A simple yet effective method has been developed to simulate macro-segregation during continuous casting. The model focuses on a thin slice moving at the casting speed, incorporating temperature and solid/liquid fraction profiles. The model incorporates micro-segregation and two key flow mechanisms: density-driven flow, governed by mass balance, and cavity-driven flow, which occurs as liquid and equiaxed crystals fill the solidification cavity forming at the center during solidification. Density-driven flow leads to positive macro-segregation near the center in both slabs and blooms, but the effect is significantly stronger in blooms. This is attributed to their higher Flow Contribution Ratio (FCR), which quantifies the relative contribution of Y-axis flow to overall flow. The higher FCR is likely influenced by greater solidification shrinkage. The cavity-driven flow model successfully explains the observed positive segregation peak at the center and the negative segregation peak at the total shrinkage location. The model's predictions closely match experimental data and provide valuable insights for optimizing casting parameters and soft reduction patterns to minimize center-segregation. With its fast computation speed, the model is well-suited for both offline analysis and real-time implementation, making it a valuable tool for research and industrial applications.

KEYWORDS: CONTINUOUS CASTING, MACRO-SEGREGATION, SHRINKAGE, CENTER-SEGREGATION, SOFT REDUCTION, DENSITY-DRIVEN FLOW, CAVITY-DRIVEN FLOW;

INTRODUCTION

Center segregation in continuous casting is influenced by several factors, including density variations [1, 2], bulging [1-4], shrinkage cavities, and liquid feeding [6, 7]. Bulging has been reported to significantly increase positive peak segregation at the center of cast products. However, its effect may be overestimated when considering the actual extent of bulging [2-4]. While previous studies have investigated macro-segregation, the specific contributions of density-driven flow and cavity-driven flow remain unclear. Additionally, inconsistencies exist in prior research regarding the relationship between density differences and segregation [2, 4, 5]. The role of shrinkage cavities as driving forces for center segregation is qualitatively well understood, but there is a lack of quantitative modeling to assess the impact of cavity-driven flow. Furthermore, the interactions among shrinkage cavities, shrinkage pores [8], and limited liquid feeding need to be verified to fully evaluate their effects on center segregation.

To address these challenges, this study introduces a

Joodong Lee, Seok Seo
Expresslab Inc., South Korea

Wonjae Cho, Eunkyu Lee, Junhyun Jo, Kyungsoo Kim
Hyundai steel, South Korea

moving-slice model that incorporates both density-driven and cavity-driven flow to analyze macro-segregation. In the density-driven flow model, macro-segregation is calculated using Y-axis velocity, which is derived from mass balance equations. In the cavity-driven flow model, the study proposes a shrinkage pore distribution approach to quantitatively evaluate center-segregation. Additionally, this study introduces the concept of the Flow Contribution Ratio (FCR), a parameter that measures the relative contribution of Y-axis flow to overall flow. By incorporating FCR, the model provides a clearer understanding of how flow dynamics influence segregation intensity. To ensure reliability, the model's predictions are validated against experimental measurements, demonstrating a strong match with observed data. This validation confirms the model's ability to accurately simulate macro-segregation behavior. By offering a comprehensive framework for analyzing segregation, this study provides valuable insights for optimizing casting processes, particularly in controlling center segregation and improving product quality.

CALCULATION PROCEDURES

Heat and solidification

The heat transfer and solidification are governed by the two-dimensional transient heat equation. The material properties depend on temperature, and the analysis considers a moving slice with a heat flux boundary condition that changes with time. Detailed discussions are provided in a separate paper by the author [9].

$$\frac{\partial}{\partial x}\left(K_x \frac{\partial T}{\partial x}\right) + \frac{\partial}{\partial y}\left(K_y \frac{\partial T}{\partial y}\right) = \rho C_p \frac{\partial T}{\partial t} \qquad [1]$$

Macro-segregation due to density change

The liquid fraction, liquid and solid concentrations, and temperature for each element are calculated, incorporating the Clyne and Kurz micro-segregation model [10], as it was found to fit best with experimental results from the continuous casting simulator at Hyundai Steel [11]. For macro-segregation analysis, a thin slice is assumed to move at the casting speed, experiencing the liquid flow caused by density change. The flow along the thickness direction contributes to macro-segregation, which can be calculated using equation 2. [3, 4]

$$\frac{\partial g_L}{\partial C_L} = -\left(\frac{1-\alpha}{1-k}\right)\left(1-\frac{V_y}{R}\right)\frac{\beta k - g_L(\beta k - 1)}{C_L} \qquad [2]$$

Here, g_L is volume fraction liquid, β is solidification shrinkage, V_y is the component of flow in the y direction, and R is the solid/liquid interface velocity. For cases involving soft reduction, V_y can be replaced by the relative velocity, $V_y - \gamma V_{SR}$, where V_{SR} is soft reduction velocity, and γ represents the efficiency of soft reduction. At each time step, the concentration of elements evolves and accumulates as they traverse the mushy zone, ultimately determining the final concentration at the end of solidification. The flow velocity, $\vec{V}$, responsible for macro-segregation is obtained by solving the following equation 3.

$$\frac{\partial \bar{\rho}}{\partial t} = -\nabla\left(\rho_L g_L \vec{V}\right) \qquad [3]$$

Here, $\bar{\rho}$ is the average density of liquid and solid. The left-hand side can be transformed as follows:

$$-\frac{\partial \bar{\rho}}{\partial t} = -\frac{\partial(\rho_L - \rho_S)}{\partial t}\cdot g_L - (\rho_L - \rho_s)\frac{\partial g_L}{\partial t} - \frac{\partial \rho_S}{\partial t} = -\frac{\partial \rho_L}{\partial g_L}\cdot\frac{\partial g_L}{\partial x}\cdot V_c g_L + (\rho_L - \rho_s)R \qquad [4]$$

Here, V_c is the casting speed, R is the solidification rate. The right-hand side can be transformed by [5] to [7]. Therefore, equation 8 can be derived, where: $\frac{d\rho_L}{dg_L}$ is defined by equation 9.

$$\nabla\rho_L \cdot g_L \vec{V} + \rho_L \nabla g_L \cdot \vec{V} + \rho_L g_L \nabla \vec{V} = \left(\frac{\partial \rho_L}{\partial x}\vec{i} + \frac{\partial \rho_L}{\partial y}\vec{j} + \frac{\partial \rho_L}{\partial z}\vec{k}\right) g_L\left(V_x\vec{i} + V_y\vec{j} + V_Z\vec{k}\right)$$

$$+\rho_L\left(\frac{\partial g_L}{\partial x}\vec{i} + \frac{\partial g_L}{\partial y}\vec{j} + \frac{\partial g_L}{\partial z}\vec{k}\right)\left(V_x\vec{i} + V_y\vec{j} + V_Z\vec{k}\right) + \rho_L g_L\left(\frac{\partial V_x}{\partial x} + \frac{\partial V_y}{\partial y} + \frac{\partial V_z}{\partial z}\right)$$

$$= \left(\frac{\partial \rho_L}{\partial g_L} g_L + \rho_L\right)\frac{\partial g_L}{\partial x} \cdot V_x + \left(\frac{\partial \rho_L}{\partial g_L} g_L + \rho_L\right)\frac{\partial g_L}{\partial y} \cdot V_y + \rho_L g_L \frac{\partial V_x}{\partial x} + \rho_L g_L \frac{\partial V_y}{\partial y} \quad [5]$$

$$\nabla\left(\rho_L g_L \vec{V}\right) = \left(\frac{\partial \rho_L}{\partial g_L} g_L + \rho_L\right)\frac{\partial g_L}{\partial x}\frac{\partial \varphi}{\partial x} + \left(\frac{\partial \rho_L}{\partial g_L} g_L + \rho_L\right)\frac{\partial g_L}{\partial y}\frac{\partial \phi}{\partial y} + \rho_L g_L \frac{\partial^2 \phi}{\partial x^2} + \rho_L g_L \frac{\partial^2 \phi}{\partial y^2} \quad [6]$$

$$\vec{V} = \nabla\phi = \frac{\partial \phi}{\partial x}\vec{i} + \frac{\partial \phi}{\partial y}\vec{j} + \frac{\partial \phi}{\partial z}\vec{k} \qquad \Rightarrow V_x = \frac{\partial \phi}{\partial x}, V_y = \frac{\partial \phi}{\partial y}, V_z = \frac{\partial \phi}{\partial z} \quad [7]$$

$$-\frac{\partial \rho_L}{\partial g_L}\frac{\partial g_L}{\partial x} V_c g_L + (\rho_L - \rho_S)R = \left(\frac{\partial \rho_L}{\partial g_L} g_L + \rho_L\right)\frac{\partial g_L}{\partial x}\frac{\partial \phi}{\partial x} + \left(\frac{\partial \rho_L}{\partial g_L} g_L + \rho_L\right)\frac{\partial g_L}{\partial y}\frac{\partial \phi}{\partial y} + \rho_L g_L \frac{\partial^2 \phi}{\partial x^2} + \rho_L g_L \frac{\partial^2 \phi}{\partial y^2} \quad [8]$$

$$\frac{d\rho_L}{dg_L} = \frac{\partial \rho_L}{\partial T}\frac{\partial T}{\partial g_L} + \sum_{i=1}^{m}\frac{\partial \rho_L}{\partial C_{Li}}\frac{\partial C_{Li}}{\partial g_L} \quad [9]$$

Where, $\frac{\partial \rho_L}{\partial T}$, $\frac{\partial \rho_L}{\partial C_{L,i}}$ is obtained from the literature [12, 13]. C_{Li} is derived from the macro-segregation model explained in equation 2. The liquid velocity, $\vec{V}$, is calculated by solving equation 8.

Center-segregation by cavity-driven flow due to solidification shrinkage

Shrinkage during solidification can result in the formation of a cavity at the slab center. When this occurs, liquid tends to flow into the cavity, causing the observed positive center-segregation. This mechanism is supported by the presence of V-segregation [4, 8]. To estimate center-segregation, the liquid filling of the central cavity is modeled, assuming the slice moves at the casting speed. The key assumptions are as follows: (1) **Shrinkage cavity formation**: The model assumes cavities form at the center due to shrinkage. (2) **Filling by liquid or equiaxed crystals**: Shrinkage cavities are filled by the flow of liquid and equiaxed crystals within the slice. (3) **Shrinkage pore formation**: Restricted liquid feeding within the mushy zone leads to the shrinkage pore formation. (4) **Initial cavity size:** The size of initial cavities in the central region is affected by the solidification rate, soft reduction, and bulging. Soft reduction decreases the central cavity, with its reduction quantified by both the soft reduction rate and reduction efficiency. Conversely, bulging results in an increase in the central cavity; thus, the bulging amount is included as indicated in equation 15. In this study, the individual contributions of soft reduction and bulging to center-segregation have not been assessed. Instead, the accuracy of current models in predicting the center-segregation profile has been verified. The influence of solidification rate on solidification shrinkage cavity is presented below. The shrinkage at each time step and the total shrinkage are described as:

$$Sh_t = \sum_{y=0}^{y_s}\left(\sqrt[3]{\rho(T_{i,t})/\rho(T_{i,t+\Delta t})} - 1\right)\cdot \Delta l, \quad Sh_{tot} = \sum_{x=0}^{x_E} Sh_t \quad [10]$$

Here, Δl represents the element thickness. The positions of y=0, y=y_s, and x=0, x=x_E are illustrated in figure 1. The density is determined by the following equation 11.

$$\rho^{\phi} = \rho_{Fe}^{\phi} + \sum k_i^{\phi} C_i^{\phi} \quad [11]$$

Here, ρ_{Fe}^{ϕ} represents the density of phase ϕ, and k_i^{ϕ}, C_i^{ϕ} are the coefficient and concentration of element i in phase ϕ, respectively. These values are obtained from the literature [12, 13]. A shrinkage cavity element is added to the top (center of the slab) of the thin slice at each time step. It is assumed that liquid flows upward from beneath the cavity,

filling it. This solute-rich liquid increases the concentration in the cavity relative to the bulk composition. As the slice moves, this process repeats, progressively enhancing center-segregation. The final center-segregation is achieved at the end of solidification. This concept of the cavity-driven flow mechanism is illustrated schematically in figure 1. In real scenarios, however, flow along the X-axis also plays a role in macro-segregation. To quantify the influence of X-axis flow, we introduce the Flow Contribution Ratio (FCR), which is defined by $V_y/(V_x + V_y)$. FCR quantifies the relative contribution of Y-axis flow (V_y) to the overall flow.

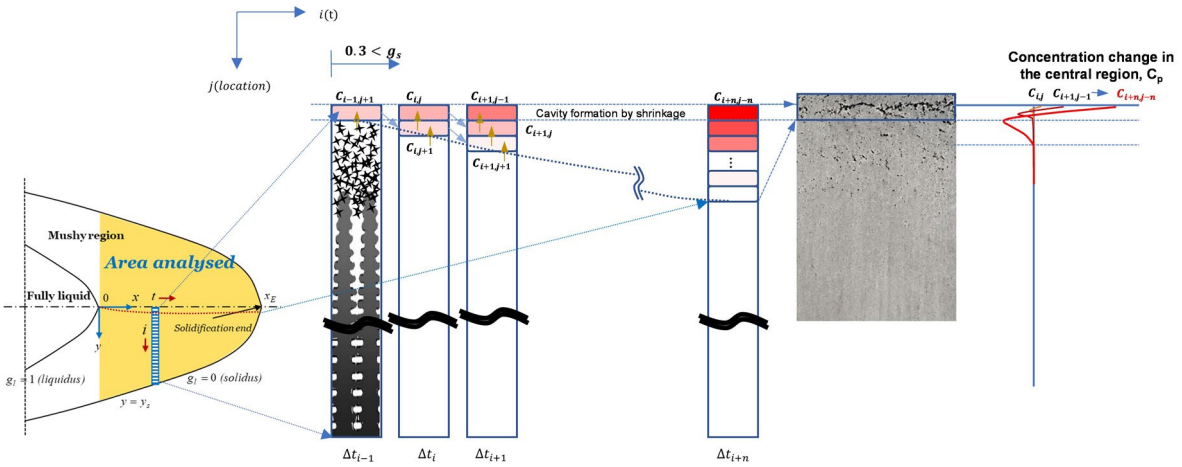

Fig.1 - Center-segregation formation by shrinkage cavity-driven flow.

While macro-segregation is directly caused by V_y, V_x can influence its intensity through a dilution effect. Physically, FCR represents the extent to which V_x mitigates macro-segregation induced by V_y. When FCR approaches 1, the influence of V_x is minimal, leading to stronger macro-segregation. Conversely, when FCR approaches 0, the dilution effect of V_x becomes dominant, significantly reducing macro-segregation. To account for this effect, FCR is multiplied by the concentration of the filling mixture at each time, as shown in Equation 15 and 16. The value of FCR can be determined by the angle of the feeding flow, which can be inferred from the V-shaped segregation observed in the slab or bloom. As the solute-rich inter-dendritic liquid fills the cavity, shrinkage pores may form at points where the liquid flow begins. While some pores are filled with liquid, others remain unfilled due to restricted liquid feeding caused by the increasing solid fraction. To validate this proposed mechanism, it is essential to measure the pore distribution in future studies. The center concentration can be calculated as following: As described by equation 12, the overall concentration of the filling mixture is represented by $C'_{i,j}$. The specific concentrations of filling liquid and solid are denoted by $C'_{l,i-1,j+1}$ and $C'_{s,i-1,j+1}$, respectively. $C_{i-1,j+1}$ indicates the concentration at the center from the previous time step (equation 13).

$$C'_{i,j} = C'_{l,i-1,j+1} g'_{l,i,j+1} + C'_{s,i-1,j+1} g'_{s,i,j+1} \quad [12]$$

$$C'_{l_{i-1,j+1}} = C_{i-1,j+1}(1 + g_{s_{i,j+1}}(\beta_i k_i - 1))^{\frac{1-k_i}{\beta_i k_i - 1}} \quad [13]$$

The fractions of the filling liquid and solid are represented by $g'_{l,i,j+1}$ and $g'_{s,i,j+1}$, respectively.

$$g'_{l,i,j+1} = \frac{\theta_{l,i,j+1} g_{l,i,j+1}}{\theta_{l,i,j+1} g_{l,i,j+1} + \theta_{ec,i,j+1} g_{s,i,j+1}} \qquad g'_{s,i,j+1} = \frac{\theta_{ec,i,j+1} g_{s,i,j+1}}{\theta_{l,i,j+1} g_{l,i,j+1} + \theta_{ec,i,j+1} g_{s,i,j+1}} \quad [14]$$

Here, $\theta_{l,i,j+1}$ represents the ratio of the filling liquid amount to the original liquid amount, while $\theta_{ec,i,j+1}$ represents the corresponding ratio for the solid phase. $\theta_{l,i,j+1}$ and $\theta_{ec,i,j+1}$ depends on the mobility of equiaxed-crystal phase, which is affected by factors such as solid fraction and the size of equiaxed-crystals [4]. In this study, only the liquid enters the cavity by assuming $\theta_{l,i,j+1}$=1 and $\theta_{ec,i,j+1}$=0. The concentration at the center location within the measured area, M, is denoted by $C_{i,j}$, as described in equation 15 and 16. This area consists of four distinct parts: (1) the initial cavity filled with solute-rich liquid and equiaxed crystal (first term of equation 16), (2) the region outside the initial cavity (second term in equation 16), (3) the initial cavity not filled (the pores or remained cavities within the initial cavity, $p_{i,j}$, and (4) the pores located outside the initial cavity, $p'_{i,j}$. These four distinct parts are represented in figure 2. The initial cavity size without soft reduction is described by $E_{i,j}$, while S_i represents the ratio of soft reduction to the cavity size. Additionally, b_i denotes the bulging amount. The concentration at the center is given by:

$When\ M \le (E_{i,j} + b_i)(1 - S_i),$

$$C_{i,j} = (FCR)C'_{i,j}(E_{i,j} + b_i)(1 - S_i)(1 - p_{i,j}) \quad [15]$$

$When\ M > (E_{i,j} + b_i)(1 - S_i),$

$$C_{i,j} = \frac{(FCR)C'_{i,j}(E_{i,j}+b_i)(1-S_i)(1-p_{i,j})}{M} + \frac{C_{i-1,j+1}(M-(E_{i,j}+b_i)(1-S_i))(1-p'_{i,j})}{M} \quad [16]$$

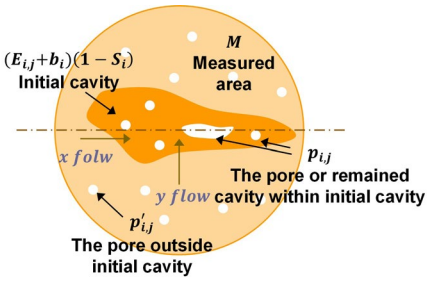

Fig.2 - Center-segregation area with four different parts.

RESULTS AND DISCUSSION

Temperature and Solidification

Figure 3 presents the results of the analysis of temperature distribution and solidification shell thickness for two casting conditions. In the first case, Steel A (slab), with a composition of 0.0594 wt% carbon and 1.179 wt% manganese, was cast at a speed of 1.1 m/min. The slab had a width of 2200 mm and a thickness of 250 mm. In the second case, Steel B (bloom), characterized by a composition of 0.2271 wt% carbon and 0.821 wt% manganese, was cast at a speed of 0.55 m/min, and had a width of 530 mm and a thickness of 390 mm

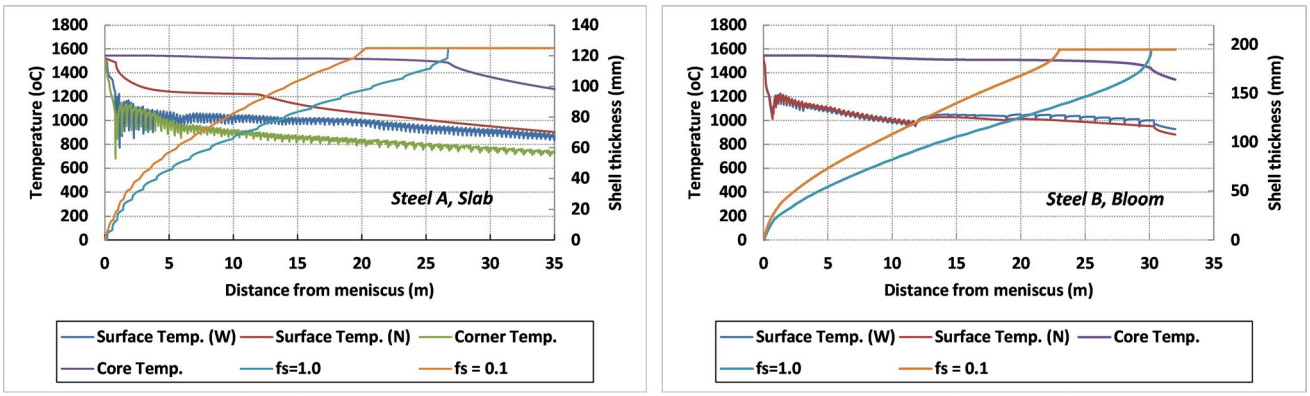

Fig.3 - Temperature and shell thickness along the distance from meniscus (Steel A: Slab, Steel B: Bloom).

Calculated liquid flow due to density change

The direction of liquid flow is depicted in figure 4, with the X-axis representing the casting direction and the Y-axis representing the thickness from the slab center to the surface. In section A (9.87mm from the center), the X flow moves toward the solidification end. This flow increases but rapidly decreases as it approaches the end of solidification in figure 4(c). The Y flow is directed toward the surface in the upper part of the caster. However, as it progresses, the flow reverses direction toward the slab center, increases in magnitude, and then diminishes near the solidification end, as depicted in figure 4(d). The maximum velocity toward the slab center develops between the center and the solidus (figure 4(e)). In the model, only the Y velocity is considered for macro-segregation calculations. In the solid/liquid region, the Y flow tends toward the center, which leads to positive macro-segregation.

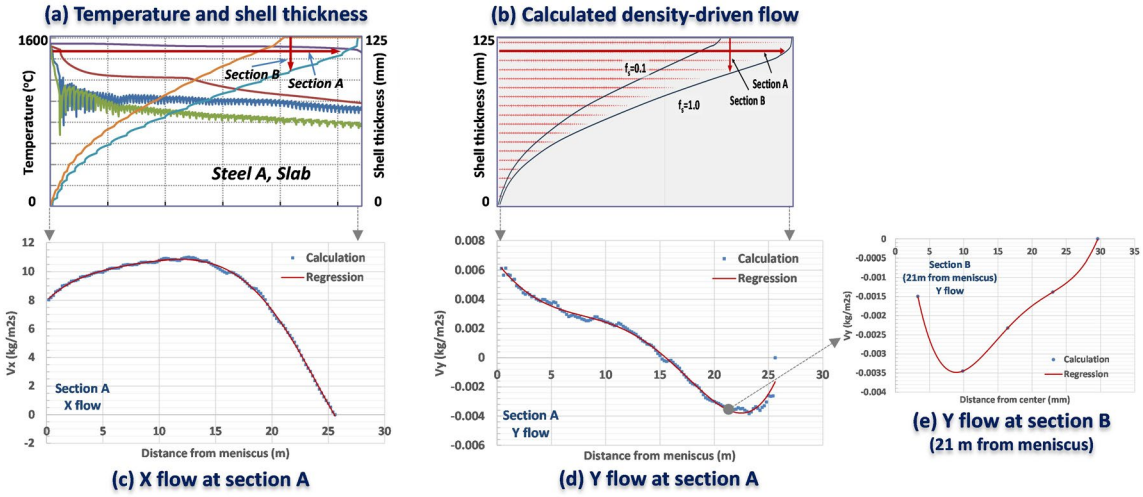

Fig.4 - The calculated results illustrate density-driven liquid flow along the casting direction (x) and thickness direction (y). Positive macro-segregation occurs only when the Y-flow's negative value moves toward the slab center, specifically between 16m and 26m (the end of solidification) from the meniscus at section A, as depicted in (d).

In real scenarios, X flow mitigates the macro- segregation effects of Y flow. To account for this, FCR is applied, as described in Section 1.3. Since FCR varies with distance in figure 5, the calculated element concentration is multiplied by FCR at each time step during macro-segregation analysis to reflect its influence. Figure 5 provides a comparative analysis of the FCR for both the slab and bloom at equivalent normalized thickness measured from their respective centers, which are 0.079 based on slab thickness and 0.086 based on bloom thickness. The bloom has a higher absolute FCR within macro-segregation region than the slab, which means that the bloom has higher relative contribution of Y flow to the overall flow than the slab, enhancing more macro-segregation. It is explained in detail in following section 2.3.

Fig.5 - Flow Contribution Ratio (FCR). Normalized thickness refers to the dimensionless measurement of thickness, calculated from the center of a slab or bloom relative to its overall thickness.

Macro-segregation due to density-driven flow

Figure 6 compares the calculated macro-segregation resulting from density changes with EPMA for the slab, and CS analysis for the bloom, respectively. The results show that slab experiences a slight increase in segregation near the center, extending up to approximately 40 mm, whereas bloom exhibits both a significantly higher level of segregation and a broader affected range, reaching up to 110 mm. This difference is likely due to variations in the length of the mushy zone. As shown in figure 3, the maximum mushy zone length (fs = 0.1 to fs = 1.0) is 27.1 mm for the slab and 57.2 mm for the bloom. This leads to significantly greater solidification shrinkage in bloom (12.2 mm) compared to the slab (4.26 mm), as indicated in figure 7. Although the bloom has a lower flow velocity due to its lower casting speed, figure 5 shows that it has higher absolute FCR values, likely due to greater solidification shrinkage, indicating weaker dilution by X-axis flow. Consequently, the higher FCR in the bloom leads to more pronounced macro-segregation near the center (figure 6). However, the density-driven flow alone cannot account for the positive center-segregation peak observed at the slab (or bloom) center. To address this, we estimate the center-segregation by modeling the filling of liquid into the center cavity.

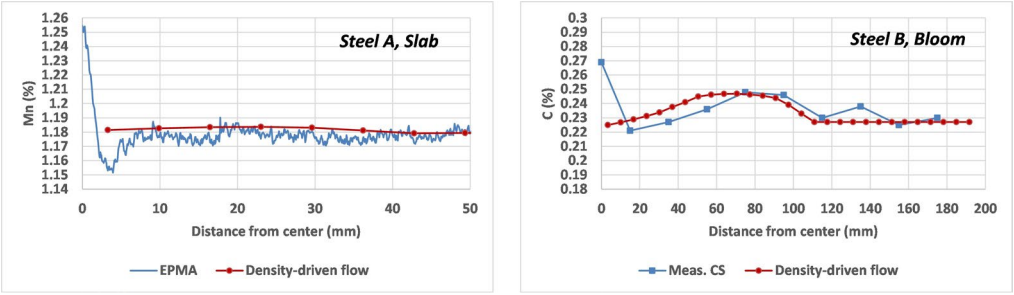

Fig.6 - Comparison of predictions based solely on density-driven flow with EPMA results for slab and CS analysis for bloom.

Center-segregation due to cavity-driven flow

Figure 7 shows the calculated concentration at the center of the slab and bloom, compared with measurements obtained using EPMA and CS analysis respectively. The first three points of calculation represent concentrations evaluated based on cavity-driven flow, while the remaining points are derived from density- driven flow analysis. The second and third points are specifically calculated using solute conservation principles as liquid fills the central cavity. Cavity-driven and density-driven flows are analyzed separately, with results combined since cavity-driven flow is central and other areas are dominated by density-driven flow. Interaction between these flows likely occurs in the transition region. Coupling both flows is necessary for improved accuracy in future analysis. Notably, the location of the lowest concentration, as measured by EPMA and CS analysis, aligns closely with the extent of shrinkage predicted by the current model.

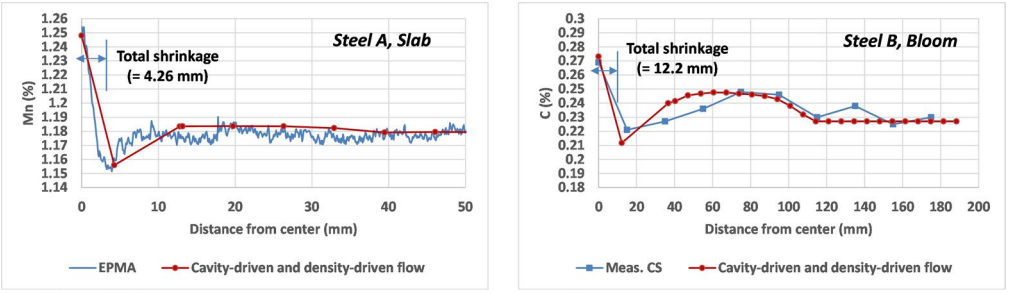

Fig.7 - Comparison of predictions based on density-driven and cavity-driven flow with measured data (EPMA for slab and CS analysis for bloom).

Negative segregation seems strongly associated with how shrinkage pores are distributed through the material's thickness. This relationship can be theoretically explained by the shrinkage behavior illustrated in figure 8. To begin with, the highest concentration of pores is expected to occur where a shrinkage cavity first develops, as this spot aligns with the greatest rate of shrinkage. As solidification advances, this point moves away from the center, accompanied by a gradual reduction in the shrinkage rate at the center, as shown in the top-left panel of figure 8. This decline in shrinkage rate may lead to a corresponding decrease in pore concentration at the central region. Ultimately, the area representing the total shrinkage thickness displays the greatest degree of negative segregation, which is attributed to the peak pore concentration. Figure 7 illustrates that the proposed cavity-driven flow model provides an effective explanation for segregation phenomena, particularly with respect to the pronounced positive peak segregation at the center and the negative peak observed at the location of total shrinkage. It is especially notable that the position of the negative segregation peak coincides with the calculated thickness of total shrinkage in the model. The findings provide substantial evidence supporting the hypothesis that negative segregation is correlated with the distribution of shrinkage pores. Additional research is required to deepen our understanding of the mechanisms governing shrinkage pore distribution and its impact on macro-segregation behavior.

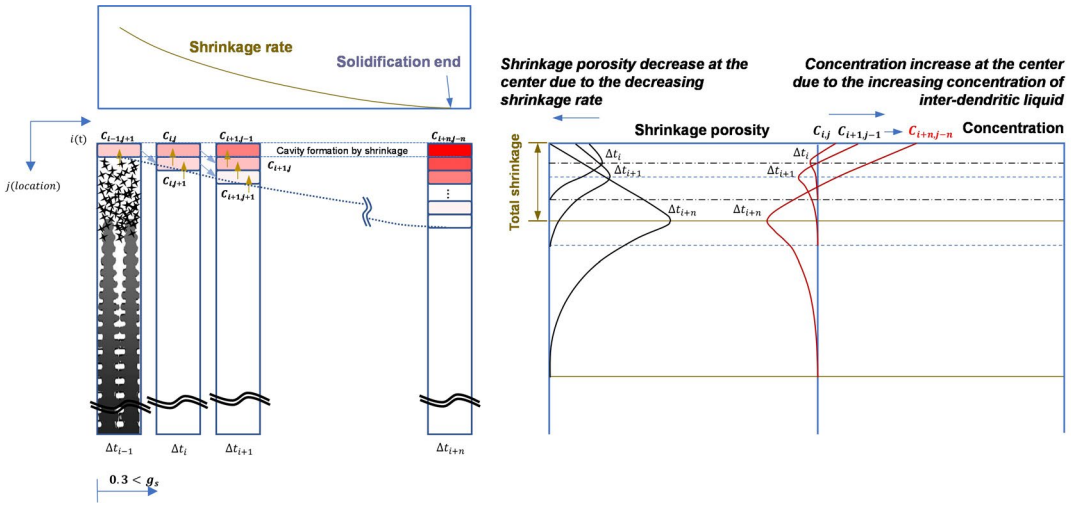

Fig.8 - Shrinkage pore distribution by shrinkage dynamics and corresponding center-segregation

CONCLUSIONS

The proposed moving-slice model effectively predicts macro-segregation, including center-segregation, in continuous casting by incorporating: (1) **Density-driven flow**, which explains the positive segregation near the center of cast products. (2) **Cavity-driven flow**, which accounts for both the positive segregation peak at the center and the negative segregation peak at the total shrinkage location. The model's predictions are validated against experimental data, confirming its reliability in capturing segregation behavior. Since both density-driven and cavity-driven flow are primarily influenced by mushy zone length and solidification shrinkage, which vary based on alloy composition, the model can theoretically be extended to other alloy systems beyond those studied. Future research will explore how pore distribution and permeability in liquid feeding affect center- segregation dynamics, further enhancing the model's applicability.

REFERENCES

[1] Donbin Jiang, Weiling Wang, Sen Luo, Cheng Ji, Miaoyong Zhu, "Mechanism of Macro segregation Formation in Continuous Casting Slab: A Numerical Simulation Study," Metall. Mater. Trans. B, vol. 48B, pp. 3120-3131, 2017
[2] F. Mayer, M. Wu, A. Ludwig. Steel Research Int, vol. 81 n. 8, pp. 660-667, 2010
[3] C. Beckermann, "Modelling of Macro segregation: Applications and future needs," Int. Materials Reviews, vol. 47, n. 5, pp. 243-261, 2002
[4] M. C. Flemings, "Our Understanding of Macro segregation: Past and Present," ISIJ International, vol. 40, n. 9, pp. 833-841, 2000
[5] Takemasa Murao, Toshiyuki Kajitani, Hideaki Yamamura, Koichi Anzai, Katsunari Oikawa, Tomoki Sawada, "Simulation of the Center-Line Segregation Generated by the Formation of Bridging," ISIJ International, vol. 54, n. 2, pp. 359-365, 2014
[6] Tadayoshi Takahashi, Masayuki Kudoh, and Kiyoshi Ichikawa, "Fluidity of the Liquid in the Solid-Liquid Coexisting Zone," Trans. Japan Inst. Metals, vol. 21, n. 8, pp. 531-538, 1980
[7] Yukinobu Natsume, Daiki Takahashi, Kasumi Kawashima, Eiji Tanigawa, Kenichi Ohsasa, "Evaluation of Permeability for Columnar Dendritic Structures by Three-dimensional Numerical Flow Analysis," ISIJ International, vol. 54, n. 2, pp. 366-373, 2014
[8] Masayuki Nakada, Kentaro Mori, Shin'ichi Nishioka, Koichi Tsutsumi, Hiroshi Murakami, Yutaka Tsuchida, "Reduction of Macro segregation by Applying a DC Magnetic Field at the Final Stage of Solidification," ISIJ International, vol. 37, n. 4, pp. 358-364, 1997
[9] Joodong Lee, Seok Seo, "Analysis of Surface Crack Initiation and Growth During Continuous Casting," AISTech 2018, May 7-10, Philadelphia, USA, 2018
[10] Young-mok Won, Brian G. Thomas, "Simple Model of Micro segregation during Solidification of Steels," Metall. Mater. Trans. A, vol. 32A, pp. 1755-1767, 2001
[11] Hyundai Steel, Experimental data provided via private communication, 2017
[12] Zarko Radovic, Milisav Lalovic, Milivoje Tripkovic, Branislav Jakic, "Forming of Positive Macro segregations during Steel Ingot Solidification," ISIJ International, vol. 39, n. 4, pp. 329-334, 1999
[13] J. Miettinen, "Calculation of Solidification-Related Thermophysical Properties for Steels," Met. Trans. B, vol. 28B, pp. 281-297, 1997

TORNA ALL'INDICE >